

How much ^{56}Ni can be produced in Core-Collapse Supernovae? : Evolution and Explosions of 30 - 100 M_{\odot} Stars

Hideyuki Umeda and Ken'ichi Nomoto

Department of Astronomy, University of Tokyo, Hongo, Bunkyo-ku, 113-0033, Japan

umeda@astron.s.u-tokyo.ac.jp; nomoto@astron.s.u-tokyo.ac.jp

ABSTRACT

Motivated by the discovery of extremely bright supernovae SNe1999as and 2006gy, we have investigated how much ^{56}Ni mass can be synthesized in core-collapse massive supernovae (SNe). We calculate the evolution of several very massive stars with initial masses $M \leq 100M_{\odot}$ from the main-sequence to the beginning of the Fe-core collapse and simulate their explosions and nucleosynthesis. In order to avoid complications associated with strong mass-loss, we only consider metal-poor stars with initial metallicity $Z = Z_{\odot}/200$. However, our results are applicable to higher metallicity models with similar C+O core masses. We find that the synthesized ^{56}Ni mass increases with the increasing explosion energy and progenitor mass. For the explosion energy of $E_{51} \equiv E/10^{51}\text{erg} = 30$, for example, the ^{56}Ni masses of $M(^{56}\text{Ni}) = 2.2, 2.3, 5.0, \text{ and } 6.6 M_{\odot}$ can be produced for the progenitors with initial masses of 30, 50, 80 and 100 M_{\odot} (or C+O core masses $M_{\text{CO}} = 11.4, 19.3, 34.0 \text{ and } 42.6 M_{\odot}$), respectively. We find that producing $M(^{56}\text{Ni}) \sim 4M_{\odot}$ as seen in SN1999as is possible for $M_{\text{CO}} \gtrsim 34 M_{\odot}$ and $E_{51} \gtrsim 20$. Producing $M(^{56}\text{Ni}) \sim 13M_{\odot}$ as suggested for SN2006gy requires a too large explosion energy for $M_{\text{CO}} \lesssim 43M_{\odot}$, but it may be possible with a reasonable explosion energy if $M_{\text{CO}} \gtrsim 60M_{\odot}$.

Subject headings: supernovae: general — supernovae: individual (SN 1999as, SN 2006gy) — nuclear reactions, nucleosynthesis, abundances

1. Introduction

Massive stars with initial masses of $M \sim 10 - 130M_{\odot}$ form iron cores at the end of their evolution, and the collapse of the iron cores triggers supernova (SN) explosions. During the

explosion explosive Si-burning produces radioactive isotope ^{56}Ni . The released energy by its decay to ^{56}Fe via ^{56}Co becomes the dominant energy source to power the optical light of most of SNe. The ejected mass of the ^{56}Ni is typically $M(^{56}\text{Ni}) = 0.07 - 0.15 M_{\odot}$ for canonical core-collapse SNe, such as SN1987A and SN1993J (e.g., Nomoto et al. 2004 for a review).

The explosion mechanism of core-collapse SNe is still uncertain. At present most popular mechanism is the delayed explosion model. In this model the gravitational energy released by the collapse is first converted into neutrinos inside a proto-neutron star, then the neutrinos heat up the matter outside to form an energetic shockwave. This mechanism may work in relatively less massive SNe of $M \lesssim 20 M_{\odot}$ to produce the normal explosion energy of $\sim 10^{51}$ ergs.

It has been recognized that there are significant numbers of core-collapse SNe, such as SN1998bw, 2002ap, 2003dh, 2003lw, that explode with much larger explosion energies than canonical SNe. These energetic SNe are called “hypernovae”, whose observational indication is the very broad line spectral feature and relatively large ejected mass of ^{56}Ni (e.g., Galama et al. 1998; Iwamoto et al. 1998). Theoretical modeling suggests that these SNe are more massive than $\sim 20 M_{\odot}$, and the compact remnant mass is large enough to exceed the maximum neutron-star mass (e.g., Nomoto et al. 2004). In modeling hypernovae we have found that the synthesized $M(^{56}\text{Ni})$ increases with explosion energies in the core-collapse SNe models with a given progenitor mass. However, there may be an upper limit for the $M(^{56}\text{Ni})$, because larger explosion energy yields a larger ^4He to ^{56}Ni ratio in the complete Si-burning region (e.g., Nakamura et al. 2001; see also Figures 5 & 6 below).

An interesting question is how much ^{56}Ni production is theoretically possible for core collapse SNe. One motivation to study this question is the observability of high-redshift SNe, that are explosions of massive stars in the early universe. In the early universe which has still very low metallicity, it is expected that the initial mass function could be top heavy or have a peak around $\sim 100 - 200 M_{\odot}$ (e.g., Nakamura & Umemura 1999; Abel et al. 2002). The stars more massive than $140 M_{\odot}$ become the pair-instability SNe (PISNe). However, we have shown in our previous papers (Umeda & Nomoto 2002, 2003, 2005; UN02, UN03, UN05 hereafter) that the nucleosynthesis patterns of very metal-poor stars do not fit to those of PISNe (also, Heger & Woosley 2002). Instead many of the stars correspond to hypernovae or energetic Fe-core collapse SNe. From precise comparisons, $M(^{56}\text{Ni})$ is estimated to be typically $0.1 - 0.4 M_{\odot}$ (Tominaga et al. 2007b; UN05) and comparable to a typical present day hypernovae such as SN1998bw. Such hypernovae can be modeled by the explosion of $25 - 50 M_{\odot}$ stars with explosion energy $\sim 10 - 40 \times 10^{51}$ ergs.

In the present days, however, there are very interesting peculiar SNe, SN1999as (Knop, R., et al. 1999) and SN2006gy (Foley et al. 2006; Ofek et al. 2007; Smith et al. 2007).

These SNe are extremely bright, and the observational and theoretical preliminary results suggest that $M(^{56}\text{Ni}) \sim 4M_{\odot}$ for SN1999as (Hatano et al. 2001) and $M(^{56}\text{Ni}) \gtrsim 13M_{\odot}$ for SN2006gy (Smith et al. 2007; Nomoto et al. 2007).

Although these estimates are preliminary, these $M(^{56}\text{Ni})$ are much more than those in previously known SNe. In Table 1, we summarize some properties of the presently known hypernova and their candidates; i.e., SN type, estimated progenitor mass, C+O core mass and the ejected $M(^{56}\text{Ni})$ obtained by spectral and light curve fitting.

As suggested by Smith et al. (2007), we have tempted to regard those extremely bright SNe as PISNe. However, the PISN models are difficult to reproduce the broad light curve of SN2006gy (Nomoto et al. 2007). In order to explain their light curves, much more explosion energy or much less ejecta mass is required than the PISNe models currently available (UN02; Heger & Woosley 2002). This provides us a motivation to study how much ^{56}Ni production is possible in the core-collapse SNe because hypernova models predict much narrower light curve than PISNe models.

The synthesized ^{56}Ni mass increases with the progenitor mass. In this paper, we thus calculate several very massive stellar models up to $100 M_{\odot}$ from the main-sequence to the beginning of the Fe core collapse. Using these models we investigate the ^{56}Ni mass production as a function of the stellar mass and explosion energy. Such very massive stars experience severe mass-loss when the stellar metallicities are large. Since the amount of mass-loss is very uncertain, we only consider such metal-poor models as $Z = 10^{-4} = Z_{\odot}/200$, for which the mass loss rate and thus the uncertainty in the stellar mass is relatively small. We note that the way of explosion, including the amount of the synthesized ^{56}Ni , is basically independent of the existence of He and H-envelopes. Therefore, most our results are applicable to higher metallicity SN models with the same C+O core progenitor masses.

The explosion mechanism of hypernovae is yet unknown. However, the inferred large remnant mass suggests that a black hole is formed and thus the explosion mechanism is different from the delayed neutrino heating model. One possible mechanism is the formation of the central black hole & accretion-disk system, and the extraction of the energy from that; this is similar to the “micro-quasar” (Paczynski 1998), “collapsar” models (MacFadyen & Woosley 1999; MacFadyen, Woosley & Heger 2001) and the jet-like explosion (Maeda & Nomoto 2003a,b). If this is the case, we need to perform 2D or 3D calculations of the explosion. For simplicity, however, we perform only 1D calculations assuming spherical symmetry. The spherical explosion model gives the upper limits to $M(^{56}\text{Ni})$ because in the jet-like explosion, for example, ^{56}Ni may be synthesized only along the jet directions.

In section 2, we describe our model and the calculation method. In section 3 we show

the results of the presupernova stellar evolutions and the synthesized $M(^{56}\text{Ni})$ during the SN explosions. Section 4 gives conclusions and discussions.

2. Model and Calculations

We calculate stellar evolution from the main-sequence to the pre- Fe-core-collapse using the same method as adopted in UN02, i.e., a Henyey type stellar evolution code which is fully coupled to a nuclear reaction network to calculate energy generation and nucleosynthesis. Some description of the code is also given in Umeda et al. (2000) and UN05.

We adopt the solar chemical composition by Anders & Grevesse (1989), the solar He abundance $Y_{\odot} = 0.27753$, and metallicity $Z_{\odot} = 0.02$. We assume that the initial helium abundance depends on metallicity Z as $Y(Z) = Y_p + (\Delta Y/\Delta Z)Z$, where primordial He abundance $Y_p = 0.247$ and $\Delta Y/\Delta Z = 1.5265$. In this paper, we only deal with $Z = 10^{-4} = Z_{\odot}/200$ models. We adopt the empirical mass loss rate (de Jager et al. 1988) scaled with the metallicity as $(Z/0.02)^{0.5}$ (Kudritzki et al. 1989).

As has been addressed by many authors (e.g., Weaver & Woosley 1993; Nomoto & Hashimoto 1988; Imbriani et al. 2001) one of the most important quantities that affect the pre-SN stellar structure and nucleosynthesis is the carbon abundance after He-burning. This quantity sensitively depends on the treatment for the core convection during He burning and the reaction rate $^{12}\text{C}(\alpha, \gamma)^{16}\text{O}$. Therefore, we take the reaction rate as a parameter. According to our previous paper, we multiply the $^{12}\text{C}(\alpha, \gamma)^{16}\text{O}$ rate of Caughlan & Fowler (1988; CF88 hereafter) by a constant factor as shown in Table 2.

As for the treatment of convection, we assume Schwarzschild criterion for convective instability and diffusive treatment for the convective mixing (Spruit 1992). For most of the models in this paper we assume relatively slow convective mixing ($f_k = 0.1$; Umeda et al. 2000). Larger f_k leads to stronger mixing of nuclear fuel, thus resulting in stronger convective shell burning. This effect leads to a smaller mass core. However, larger f_k leads to less carbon fraction after He-burning, which instead leads to a larger core. Therefore, it is not simple to predict the final outcome as a function of the parameter f_k .

Once pre-SN progenitor models are obtained, we simulate their SN explosions with a 1D piecewise parabolic method (PPM) code by putting explosion energy into some mesh points just below the mass cut. Here we do not specify the explosion mechanism and assume spherical symmetry for simplicity because the hypernova mechanism is highly uncertain. The detailed nucleosynthesis during the explosion is calculated by postprocessing as described in UN02.

3. Results

3.1. Pre-Supernova Evolution

In Table 2, we summarize the parameters and some properties of our pre-SN progenitor models. The first three columns are the initial mass, convection parameter f_k and the factor multiplied to the CF88 $^{12}\text{C}(\alpha, \gamma)^{16}\text{O}$ rate. The next six columns are the pre-SN progenitor final-mass with mass-loss (M_f), He core mass, C+O core mass, C/O mass fraction after He burning, Fe core mass and the binding energy E_{bin} of the layer above the Fe-core, respectively. Here the He, C+O and Fe core masses are defined by the mass coordinate where the fractions of hydrogen and helium are $X(\text{H}) < 10^{-3}$, $X(\text{He}) < 10^{-3}$ and electron mole fraction $Y_e < 0.49$ in the progenitor models, respectively.

The total amount of mass-loss is larger for more massive stars. However, with this low metallicity the total lost mass is not so large even for $M = 100M_\odot$ and a large fraction of the hydrogen envelope still remains. Therefore, such a star becomes SN II unless it is in a binary system with its envelope being stripped off by binary interaction.

In the models shown in this paper, the Fe core mass is larger for more massive stars. This is usually the case but not always, because the Fe core mass depends on the C/O ratio after He-burning. For a larger C/O ratio, convective C-burning is stronger, thus forming a smaller Fe-core (e.g., Nomoto & Hashimoto 1988). The C/O ratio is generally smaller for more massive stars, because the $^{12}\text{C}(\alpha, \gamma)^{16}\text{O}$ reaction is more efficient than the 3α reactions at higher temperatures and lower densities. However, the C/O ratio also strongly depends on the convective mixing at the end of He-burning.

The evolutions of $M \lesssim 100M_\odot$ stars are all similar in the sense that all these stars form Fe-cores to initiate Fe-core collapse. Nevertheless, we find a difference in the evolution of the stars more massive than $80M_\odot$. These stars experience “pulsations” at the end of Si-burning (see also Heger et al. 2003).

In Figure 1 we show the evolution of the central density and temperature for the 30 and $90M_\odot$ models. It is well known that a more massive star has a larger specific entropy at the center. Thus the temperature of the more massive star is higher for the same density. Along with this fact we find that the central temperature and density evolution is very different between the 30 and $90M_\odot$ models during the “Si”-burning stage, which takes place around the temperature $T_9 = 2.5 - 4$. Here “Si” includes not only ^{28}Si but also all the elements heavier than Si and lighter than Fe. The central temperature and density of the $90M_\odot$ model oscillate several times. This is because in such a massive star radiation pressure is so dominant that the adiabatic index of the equation of state is close to $\Gamma \sim 4/3$, and thus

the inner core of the stars easily expands with the input of the nuclear energy released by “Si”-burning. Once it expands, the temperature drops suddenly, central “Si”-burning stops and the stellar core turns into contraction. Since only a small amount of “Si” is burnt in each cycle, these pulsations occur many times. Note that as shown in Figure 1 the density - temperature track is very close to (but outside of) the electron-positron pair-instability region” where $\Gamma < 4/3$ (e.g., Barkat et al. 1967).

A similar type of oscillations has been reported for metal-poor stars of $100M_{\odot} \gtrsim M \gtrsim 140M_{\odot}$ in Heger et al. (2003) as ”Pulsational PISNe”. They discussed that these stars encounter pair instability, leading to violent pulsations, but not complete disruptions. Each pulse can have up to several 10^{51} ergs, and only outer layers of the star are expelled. In our model for the $80 - 100M_{\odot}$ stars we have not found such mass-loss probably because the mass-range is lower and also we have attached H-envelope that absorbs and relieves the pulsations.

We have found from the study of $80-100M_{\odot}$ stars that the number of the oscillations depends on the convective parameter f_k : larger f_k increases the number of the oscillation. This is because for a larger f_k fresh Si is more efficiently mixed into the central region, which increase the lifetime of this stage. The amplitude of the temperature and density variation is larger for more massive stars, which suggests that more and more drastic oscillations could occur for stars of $M > 100M_{\odot}$. During this stage, the specific entropy at the center is reduced (or density is increased) and the Fe-core, which is defined as a region with $Y_e \leq 0.49$, grows. However, the pulsations does not much affect on $M(^{56}\text{Ni})$.

3.2. Pre-supernova Density Structure

As described in the next subsection, the amount of produced ^{56}Ni is closely related to the density structure, more specifically the enclosed mass (M_r) - radius (r) relation, of the pre-SN progenitors, where M_r is the mass contained within a sphere of radius r . Figure 2 shows this $M_r - r$ relation for our progenitor models. For reference, in Figure 3 and 4 we show distributions of density ρ and electron mole fraction Y_e , respectively. We see that the $M_r - r$ curve is steeper for more massive stars, which means more massive stars are more centrally concentrated. In some cases, however, less massive stars have a steeper $M_r - r$ relation if the C/O ratio after the He burning is smaller, which leads to a larger core mass.

3.3. Explosive Nucleosynthesis of ^{56}Ni

The products of explosive burning are largely determined by the maximum temperature behind the shock, T_s . Material which experiences $T_{s,9} \equiv T_s/10^9 \text{ K} > 5$ undergoes complete Si-burning, forming predominantly ^{56}Ni . The region after the shock passage is radiation dominant, so that we can estimate the radius of the sphere in which ^{56}Ni is dominantly produced as

$$R_{\text{Ni}} \sim 3700 E_{51}^{*1/3} \text{ km}, \quad (1)$$

which is derived from $E^* = 4\pi R_{\text{Ni}}^3 a T_s^4/3$ with $T_{s,9} = 5$ (e.g., Thielemann et al. 1996). Note that the deposited energy E^* is approximately equal to the sum of the explosion energy E_{exp} and the binding energy ($E_{\text{bin}} > 0$) of the progenitor, i.e., $E^* \simeq E_{\text{exp}} + E_{\text{bin}}$.

We show in Figure 2 the radii which correspond to $E_{51}^* = 1, 10, 50$ and 100 , where the solid circles on the $M_r - r$ curves indicates the outer edge of the core, i.e., the masses of Fe-cores. This figure suggests that the ^{56}Ni synthesis is larger for larger E^* and for the models with steeper $M_r - r$ curves, i.e., more massive stars. The mass between the outer edge of the Fe-core and $r = R_{\text{Ni}}$ gives the crude upper-limit to $M(^{56}\text{Ni})$ in the ejecta. This is an upper-limit because the mass-cut, that divides the compact remnant and ejecta, can be far above the Fe-core, and also the mass fraction of ^{56}Ni in the complete Si-burning region can be significantly smaller than 1.0 especially for the very energetic explosion (see Figure 5 & 6 and discussion below).

In order to obtain the synthesized $M(^{56}\text{Ni})$ more precisely, we perform explosion simulation using the 1D PPM code and detailed postprocess nucleosynthesis calculations (see e.g., UN05). Figures 5 & 6 show examples of the results obtained in this way. These are the post-explosion abundance distributions in the $50M_\odot$ and $100 M_\odot$ models for the explosion energy of $E_{51} = 30$ (left) and $E_{51} = 100$ (right), respectively. As shown in these figure, for a more energetic explosion, α -rich freezeout is stronger so that the mass fraction ratio of $^4\text{He}/^{56}\text{Ni}$ increases in the complete Si-burning region.

The results are summarized in Table 3. Here, the models A-F are the same as in Table 2. For each model, the results with various explosion energies are shown. The upper limit of the ^{56}Ni mass is shown as $^{56}\text{Ni}_{\text{up}}$ in the last column. This is the upper limit, because the mass-cut is assumed to be equal to the Fe-core mass given in Table 2. In reality, though it depends on the model assumptions¹ the mass-cut is likely larger than the Fe-core mass, then

¹If the explosion is strictly spherical and the location of the energy deposition is uniquely determined, we can uniquely determine the mass-cut as a function of E_{exp} . However, in an aspherical model or in a jet-like explosion with energy injection by continuous jets (e.g., Tominaga et al. 2007a), the "effective mass-cut"

the ejected ^{56}Ni mass could be smaller. $^{56}\text{Ni}_{\text{up}}$ is also summarized in Figure 7.

In Table 3 we show the compact remnant mass M_{rem} for reference. M_{rem} corresponds to the mass-cut when $0.07 M_{\odot}$ of ^{56}Ni is ejected. If $M(^{56}\text{Ni})$ is larger, therefore, the remnant mass would be smaller than M_{rem} shown in Table 3.

In the 7 and 8th columns in Table 3, we also show $M(^{56}\text{Ni})$ (almost exactly the same as the ejected Fe mass for these low metallicity models) when the mass ratios of Mg/Fe and O/Fe are the solar ratios, i.e., when $[\text{Mg}/\text{Fe}] = 0$ and $[\text{O}/\text{Fe}] = 0$, respectively. We show these quantities, because in the observations of metal-poor halo stars, most stars have the abundance of $[\text{Mg}/\text{Fe}] \geq 0$ and $[\text{O}/\text{Fe}] \geq 0$. This means that if SNe yield $[\text{Mg}/\text{Fe}] < 0$ or $[\text{O}/\text{Fe}] < 0$, or producing larger $M(^{56}\text{Ni})$ than in the 7 and 8th columns, such SNe should not be dominant in the early Galaxy. We note that if we constrain the ejecta abundances as $[\text{O}/\text{Fe}] \geq 0$, ^{56}Ni ejection of more than $3M_{\odot}$ is not possible for all the models considered in this paper.

We, however, should make a caution that the O and Mg yields from massive stars depend on the treatment of convection (e.g., f_k) and the adopted $^{12}\text{C}(\alpha, \gamma)^{16}\text{O}$ reaction rate. The model dependency of O yield would be small, at most a factor of 2, but that of Mg yield would be much larger and the yield can be a factor of 5 different at most. Generally the Mg yield increases when the C/O ratio after the He-burning is larger because Mg is the C-burning product.

We find from Table 3 that if relatively less massive SNe ($M \lesssim 30M_{\odot}$) produce ^{56}Ni as much as $2 M_{\odot}$, the ejecta is too Fe-rich to be compatible with metal-poor star abundance. On the other hand, the ejection of $M(^{56}\text{Ni}) \sim 2M_{\odot}$ from such massive stars as $M \gtrsim 80M_{\odot}$ does not contradict with the abundance of metal-poor stars.

We note that large $M(^{56}\text{Ni})$ ($\gtrsim 4M_{\odot}$) models are quite energetic, so the Zn/Fe ratios in the ejecta are relatively large, exceeding the solar ratio. This is a distinctive feature from any PISNe models which do not produce large Zn/Fe (UN02). In the energetic explosions Co/Fe ratios are also relatively high. However, as shown in UN05, the Co/Fe ratio is not much enhanced for $Y_e \lesssim 0.5$ even for the energetic explosions. In the present models, indeed, the Co/Fe ratios are less than the solar value. More detailed study about nucleosynthesis and its parameter dependences are given elsewhere.

may not simply the function of E_{exp} .

4. Conclusions and Discussions

Motivated by the discovery of unusually bright SNe 2006gy and 1999as, we have investigated how much $M(^{56}\text{Ni})$ can be synthesized by core-collapse massive SNe with the initial mass of $M \leq 100M_\odot$. Observed properties of SN1999as and 2006gy suggest that the ejected ^{56}Ni masses are $M(^{56}\text{Ni}) \sim 4M_\odot$ (Hatano et al. 2001) and $13 M_\odot$ (Nomoto et al. 2007). Previously the only known SNe model that can produce such a large $M(^{56}\text{Ni})$ is the PISNe which are the explosion of $140 - 300M_\odot$ stars. However, the light curves of PISNe may be too broad to reproduce the observed light curves of SNe1999as and 2006gy, suggesting that a less massive star explosion (Nomoto et al. 2007).

We, therefore, have calculated the evolution of several very massive stars with the initial masses of $M \leq 100M_\odot$ from the main-sequence to just before the Fe-core collapse. In order to minimize the uncertainty in the mass-loss, we have adopted low-metal ($Z = Z_\odot/200$) models throughout this paper. However, most results, especially the estimate of the ejected masses of ^{56}Ni and ^{16}O , are applicable to higher metallicity models with similar C+O core masses. Using these newly calculated progenitor models, we simulated the SN explosion of such massive stars and calculated the mass of the synthesized ^{56}Ni , and other elements.

We find that the $M \gtrsim 80M_\odot$ stars “pulsate” during the central Si-burning stages. The existence of this stage makes the lifetime of the stars longer and makes the Fe-core grow. However, the Fe-core growth during this stage is not the main reason why these massive stars can produce such large $M(^{56}\text{Ni})$. In this sense the existence of this stage is not critical for the production of the large $M(^{56}\text{Ni})$.

We have shown that the synthesized $M(^{56}\text{Ni})$ mass increases with the increasing explosion energy, E_{exp} , and the progenitor mass M . Among them the effect of M is more important than the energy because more massive stars tend to have steeper $M_r - r$ curves in the density structure of the progenitors, so that $M(^{56}\text{Ni})$ increases steeply with M for the same E_{exp} . Larger E_{exp} leads to a larger ^{56}Ni producing region according to the Equation (1); however, this also leads to a smaller Ni/He ratio in that region. As a result, a large E_{exp} does not result in so large $M(^{56}\text{Ni})$. For $E_{51} = 30$, $M(^{56}\text{Ni}) = 2.2, 2.3, 5.0,$ and $6.6 M_\odot$ can be produced for $M = 30, 50, 80$ and $100 M_\odot$, respectively, or for C+O core masses of $M_{\text{CO}} = 11.4, 19.3, 34.0$ and $42.6 M_\odot$, respectively.

It is possible to produce $M(^{56}\text{Ni}) \sim 4M_\odot$ as seen in SN1999as if $M_{\text{CO}} \sim 34M_\odot$ and $E_{51} \gtrsim 20$. On the other hand, producing $M(^{56}\text{Ni}) \gtrsim 13M_\odot$ as seen in SN2006gy is challenging for core collapse SN models if $M_{\text{CO}} < 43M_\odot$. In the present study, the most massive model has $M_{\text{CO}} = 42.6 M_\odot$. For this model, the explosion energy of $E_{51} \sim 200$ is required to produce $M(^{56}\text{Ni}) \sim 13M_\odot$ but such E_{51} may be unrealistically large, although there is no

observational constraints.

Nevertheless, we should note that if we simply extrapolate our results to more massive stars up to $M \sim 130M_{\odot}$, M_{CO} is as large as $60M_{\odot}$. Such a model would undergo core-collapse and produce $M(^{56}\text{Ni}) \sim 13M_{\odot}$ without too large explosion energy. Currently we are constructing such an extreme model, and will present the results in a forth coming paper. We are also studying very massive stars above $300M_{\odot}$ for which much study has not been done yet. Those stars may be too heavy to explode as PISNe and form blackholes (e.g., Fryer et al. 2001). The collapse of these stars may or may not accompany aspherical mass ejection and potentially eject $\sim 10M_{\odot}$ ^{56}Ni (Ohkubo et al. 2006), though the stellar metallicities must be very low in order to leave sufficiently massive cores.

We would like to thank J. Deng and N. Tominaga for useful discussions. This work has been supported in part by the grant-in-Aid for Scientific Research (18104003, 18540231) and the 21st Century COE Program (QUEST) from the JSPS and MEXT of Japan.

REFERENCES

- Abel, T., Bryan, G. L., & Norman, M. L. 2002, *Science* 295, 93
- Anders, E., & Grevesse, N. 1989, *Geochim.Cosmochim.Acta*, 53, 197
- Barkat, Z., Rakavy, G., & Sack, N. 1967, *Phys. Rev. Lett.*, 18, 379
- Caughlan, G. & Fowler, W. 1988, *Atomic Data Nucl. Data Tables*, 40, 283
- de Jager, C., Nieuwenhuijzenm, H., & van der Hucht, K. 1988, *A&AS*, 72, 259
- Foley, R. J. Li, W., Moore, M., Wong., D. S., Pooley, D., & Filippenko, A. V. 2006, *CBET*, 695, 1
- Fryer, C. L., Woosley, S. E., & Heger, A. 2001, *ApJ*, 550, 372 & Filippenko, A. V. 2006, *CBET*, 695, 1
- Galama, T. J., et al. 1998, *Nature*, 395, 670
- Hatano, K., Branch, D., Nomoto, K., Deng, J., Maeda, K., Nugent, P., & Aldering, G. 2001, *BAAS*, 33, 838
- Heger, A., & Woosley, E. 2002, *ApJ*, 567, 532

- Heger, A., Fryer, C. L., Woosley, E., Langer, N., & Hartmann, D. H. 2003, *ApJ*, 591, 288
- Imbriani, G., Limongi, M., Gialanella, L., Terrasi, F., Straniero, O., & Chieffi, A. 2001, *ApJ*, 558, 903
- Iwamoto, K., et al. 1998, *Nature*, 395, 672
- Iwamoto, K., et al. 2000, *ApJ*, 534, 660
- Knop, R., et al. 1999, *IAUC*, 7128
- Kudritzki, R., Pauldrach, A., Puls, J., & Abbott, D. 1989, *A&A*, 219, 205
- MacFadyen, A. I., & Woosley, S. E. 1999, *ApJ*, 524, 262
- MacFadyen, A. I., Woosley, S. E., & Heger, A. 2001, *ApJ*, 550, 410
- Maeda, K., & Nomoto, K. 2003a, *ApJ*, 598, 1163
- Maeda, K., & Nomoto, K. 2003b, *Prog. Theor. Phys. Suppl.*, 151, 211
- Mazzali, P. A., et al. 2002, *ApJ*, 572, L61
- Mazzali, P. A., et al. 2003, *ApJ*, 599, L95
- Nakamura, F., & Umemura, M. 1999, *ApJ*, 515, 239
- Nakamura, T., Umeda, K., Iwamoto, K., Nomoto, K., Hashimoto, M., Hix, W.R., Thielemann, F.-K. 2001, *ApJ*, 550, 880
- Nomoto, K., & Hashimoto, M. 1988, *Phys. Rep.*, 163, 13
- Nomoto, K., Maeda, K., Mazzali, P.A., Umeda, H., Deng, J., & Iwamoto, K. 2004, in *Stellar Collapse*, ed. C.L. Fryer (Dordrecht: Kluwer), 277
- Nomoto, K., Tominaga, N., Tanaka, M., Maeda, K., & Umeda, H. 2007, in *Supernova 1987A: 20 Years After–Supernovae and Gamma-Ray Bursters*, eds. S. Immler, et al. (New York: American Institute of Physics), in press (arXiv:0707.2187)
- Ofek, E. O., et al. 2007, *ApJ*, 659, L13
- Ohkubo, T., Umeda, H., Maeda, K., Nomoto, K., Suzuki, T., Tsuruta, S., & Rees, M. J. 2006, *ApJ*, 645, 1352
- Paczynski, B. 1998, *ApJ*, 494, L45

- Smith, N., et al. 2007, ApJ, submitted (astro-ph/0612617)
- Spruit, H. C. 1992, A&A, 253, 131
- Tominaga, T., Maeda, K., Umeda, H., Nomoto, K., Tanaka, M., Iwamoto, N., Suzuki, T., & Mazzali, P. 2007a, ApJ, 657, L77
- Tominaga, T., Umeda, H., & Nomoto, K. 2007b, ApJ, 660, 516
- Thielemann, F.-K., Nomoto, K., & Hashimoto, M. 1996, ApJ, 460, 408
- Umeda, H., Nomoto, K., & Nakamura, T. 2000, in *The First Stars*, ed. A. Weiss, T. Abel, & V. Hill (Berlin: Springer), 150 (astro-ph/9912248)
- Umeda, H., & Nomoto, K. 2002, ApJ, 565, 385 (UN02)
- Umeda, H., & Nomoto, K. 2003, Nature, 422, 871 (UN03)
- Umeda, H., & Nomoto, K. 2005, ApJ, 619, 427 (UN05)
- Weaver, T.A. & Woosley, S.E. 1993, Phys. Rep., 227, 665

Table 1. Properties of hypernovae and their candidates.

Name	Type	E_{51}	M_{ini}/M_{\odot}	$M_{\text{C+O}}/M_{\odot}$	$M(^{56}\text{Ni})/M_{\odot}$	Reference
SN1997ef	Ic	~ 20	~ 35	10.0	0.15	Iwamoto et al. 2000
SN1998bw	Ic	~ 40	~ 30	13.8	0.5	Iwamoto et al. 1998
SN2002ap	Ic	~ 7	~ 21	3.3	0.10	Mazzali et al. 2002
SN2003dh	Ic	$\sim 30 - 50$	$\sim 35 - 40$	4.5	0.35	Mazzali et al. 2003
SN1999as	Ic	$\sim 20 - 50$	$\sim 60 - 80$	$\sim 20 - 30$	4	Hatano et al. 2001
SN2006gy	Ib/c	?	?	?	$\gtrsim 13$	Tominaga et al. 2007
SN1987A	II	1	$\sim 18 - 20$	3	0.07	Nomoto et al. 2004

Note. — Supernova name, type, expected explosion energies in 10^{51} erg, initial progenitor masses, C+O core masses, ejected ^{56}Ni masses, and the references are shown. One canonical SN (1987A) is also shown for comparison.

Table 2. Parameters and properties of the pre-SN models.

Model	M	f_k	CF88 \times	M_f	$M(\text{He})$	$M(\text{CO})$	C/O	$M(\text{Fe})$	E_{bin}
	20	0.05	1.4	19.94	6.76	4.39	0.19/0.80	1.51	1.63
	20	0.10	1.7	19.93	6.45	5.29	0.16/0.83	1.55	1.38
A	25	0.10	1.0	24.87	8.35	6.33	0.29/0.70	1.52	1.83
B	30	0.10	1.0	29.61	13.1	11.4	0.30/0.68	1.86	1.87
C	50	0.50	1.0	48.55	21.8	19.3	0.16/0.79	2.21	3.67
D	80	0.10	1.0	75.81	36.4	34.0	0.20/0.74	2.75	5.46
E	90	0.50	1.3	83.53	37.4	36.5	0.087/0.82	3.15	4.73
F	100	0.10	1.0	83.14	46.5	42.6	0.23/0.72	3.22	7.19

Note. — Each column is the initial mass (M), convection parameter (f_k), the factor multiplied to the CF88 $^{12}\text{C}(\alpha, \gamma)^{16}\text{O}$ rate, pre-SN progenitor mass with mass-loss (M_f), He core mass, C+O core mass, C/O mass fraction after He burning, Fe-core mass and the binding energy E_{bin} . Here, all masses are shown in the units of M_{\odot} and the energy is in 10^{51} erg. These models are all for the metallicity $Z = Z_{\odot}/200$.

Table 3. The masses of Mg, O and upper mass limits of the ^{56}Ni in the ejecta of core-collapse SNe as a function of progenitor mass and explosion energy.

Model	M	E_{51}	M_{rem}	Mg	O	$^{56}\text{Ni}_{[\text{Mg}/\text{Fe}]=0}$	$^{56}\text{Ni}_{[\text{O}/\text{Fe}]=0}$	$^{56}\text{Ni}_{\text{up}}$
A	25	1	2.11	0.14	3.50	0.34	0.46	0.56
B	30	1	2.60	0.41	5.45	0.98	0.72	0.69
		10	3.57	0.41	4.68	0.98	0.62	1.43
		20	4.25	0.36	4.27	0.86	0.56	1.83
		30	4.77	0.31	3.86	0.75	0.51	2.19
		50	5.60	0.26	3.36	0.62	0.44	2.52
C	50	1	2.46	0.79	12.52	1.90	1.65	0.83
		10	4.22	0.73	11.67	1.77	1.54	1.48
		30	5.44	0.79	10.73	1.91	1.42	2.28
		50	6.26	0.80	9.96	1.94	1.32	2.74
		70	6.90	0.80	9.49	1.92	1.25	2.97
		100	7.62	0.78	8.91	1.87	1.18	3.19
D	80	150	8.62	0.76	8.16	1.82	1.08	3.60
		1	6.08	1.41	18.71	3.40	2.47	2.14
		10	8.00	1.35	17.45	3.25	2.30	3.36
		30	10.61	1.28	15.31	3.09	2.02	4.99
		50	11.89	1.20	14.33	2.89	1.89	5.74
		60	12.24	1.17	14.07	2.82	1.86	6.06
E	90	100	15.04	0.88	12.09	2.11	1.60	7.86
		1	6.08	0.38	20.59	0.92	2.72	1.85
		10	7.82	0.36	19.69	0.86	2.60	2.69
		20	9.42	0.33	18.67	0.80	2.46	3.51
		30	10.75	0.31	17.84	0.74	2.36	4.19
		50	11.75	0.28	17.01	0.68	2.25	4.85
		70	13.07	0.26	16.00	0.62	2.11	5.78
		110	14.71	0.23	14.87	0.55	1.96	6.97
F	100	1	8.74	1.58	22.41	3.81	2.96	3.34
		30	14.22	1.34	19.27	3.34	2.54	6.64
		70	17.62	1.38	16.67	3.33	2.20	8.78
		100	19.81	1.28	15.31	3.08	2.02	10.17
		210	24.43	0.83	12.50	2.00	1.65	13.49

Note. — Models A-F are the same as in Table 2. Columns 4 to 9 are the following masses in units of M_{\odot} : (4) the remnant mass for the case of $0.07M_{\odot}$ ^{56}Ni ejection (M_{rem}/M_{\odot}), (5, 6) the total Mg and O masses in the ejecta, (7, 8) the ^{56}Ni masses when the ejecta has the solar abundance ratios for Mg/Fe and O/Fe ($^{56}\text{Ni}_{[\text{Mg}/\text{Fe}]=0}$ and $^{56}\text{Ni}_{[\text{O}/\text{Fe}]=0}$), respectively, and (9) the upper limit to the ejected ^{56}Ni mass when the mass-cut is set just above the Fe-core shown in Table 2 ($^{56}\text{Ni}_{\text{up}}$) as a function of progenitor mass M and explosion energy $E_{51} \equiv E/10^{51}$ erg.

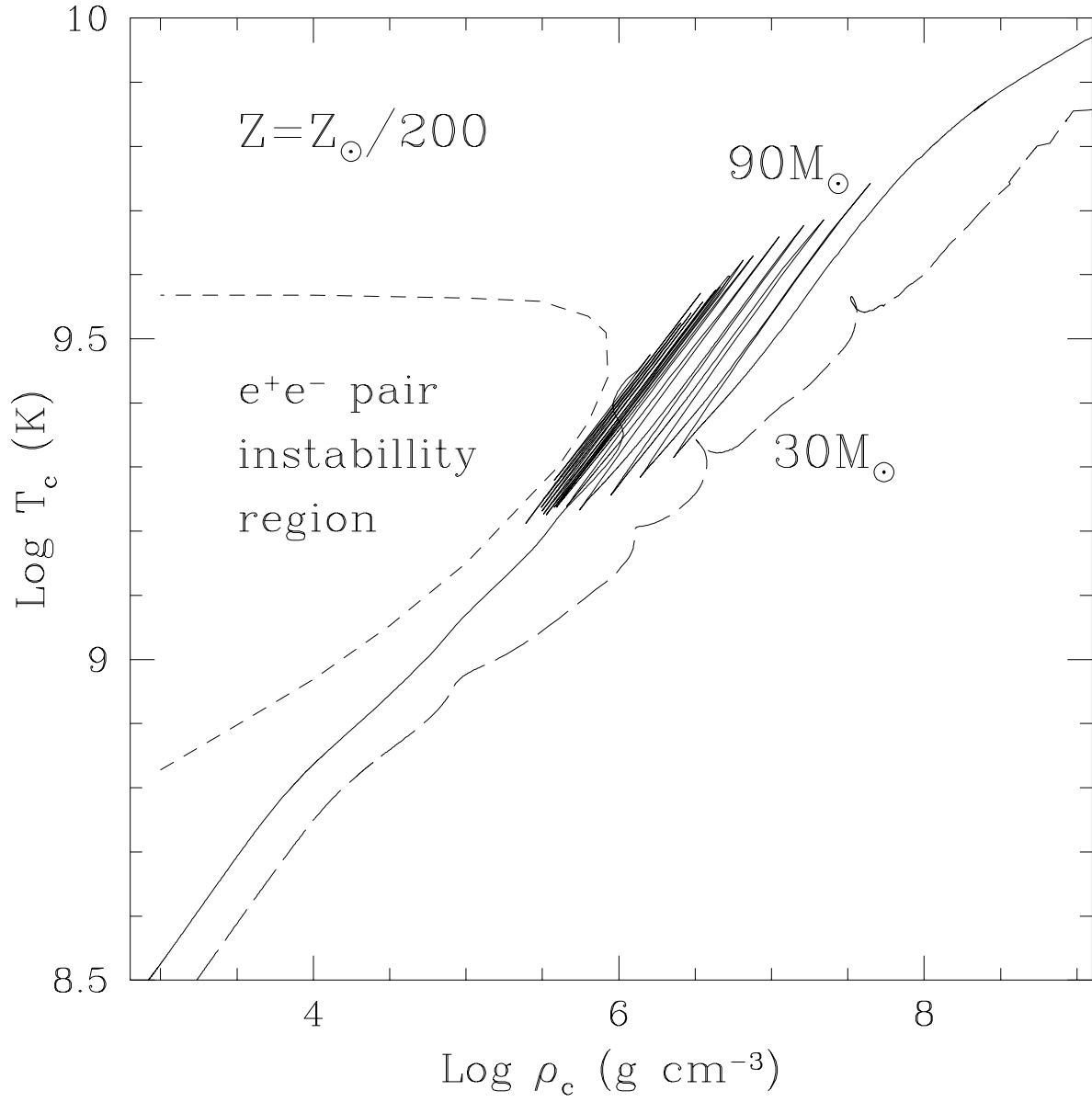


Fig. 1.— Evolution of the central density and temperature for the 30 and $90M_\odot$ models.

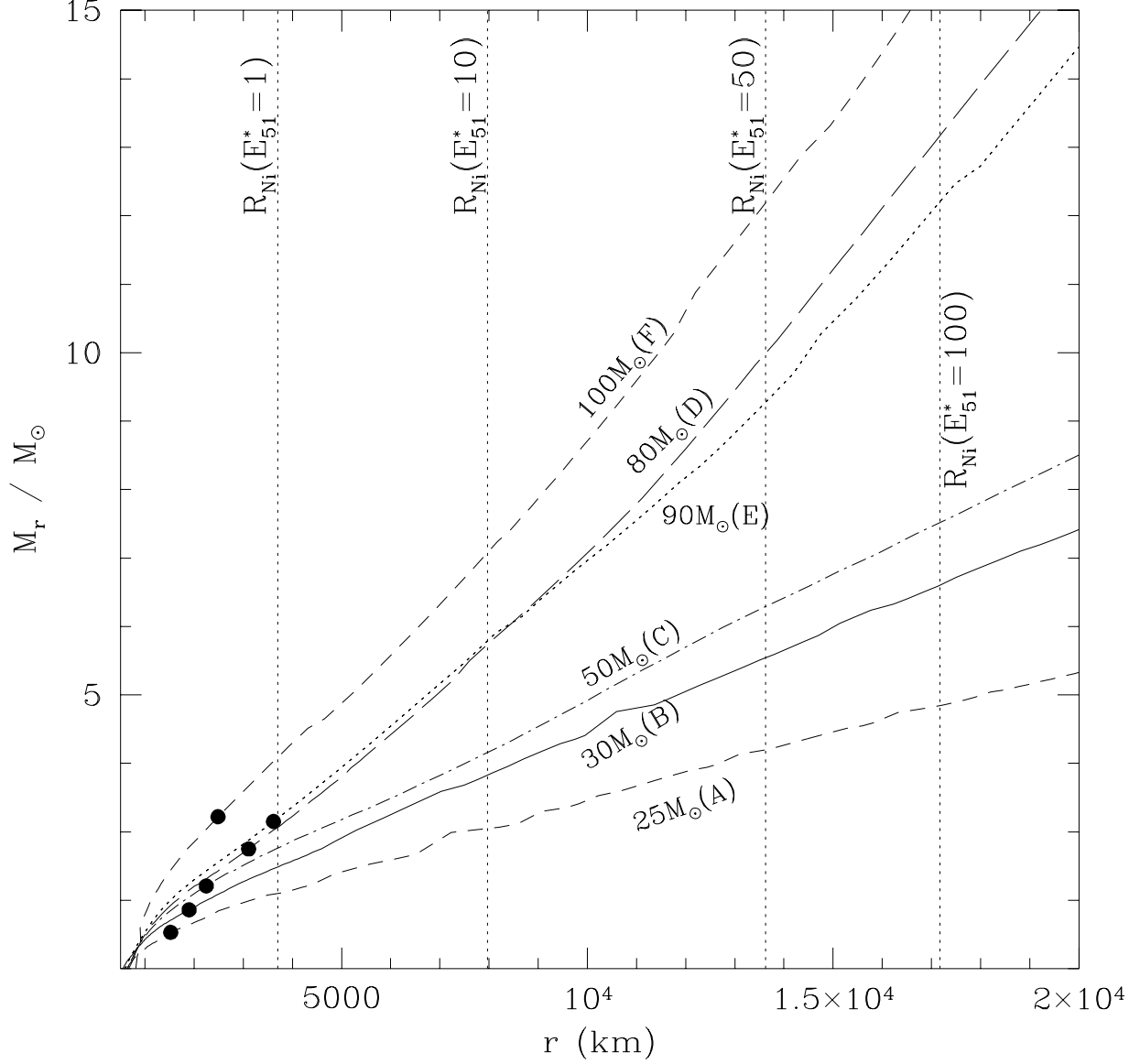


Fig. 2.— The enclosed mass (M_r) - radius relation of our pre-SN progenitors. The parameters and some properties of the models A-F are shown in Table 2. For each model the location of the top of the Fe-core is shown by a filled circle. R_{Ni} is the upper radius for the region where Ni^{56} is dominantly produced as a function of the deposited energy E^* given by the Equation (1) in the text.

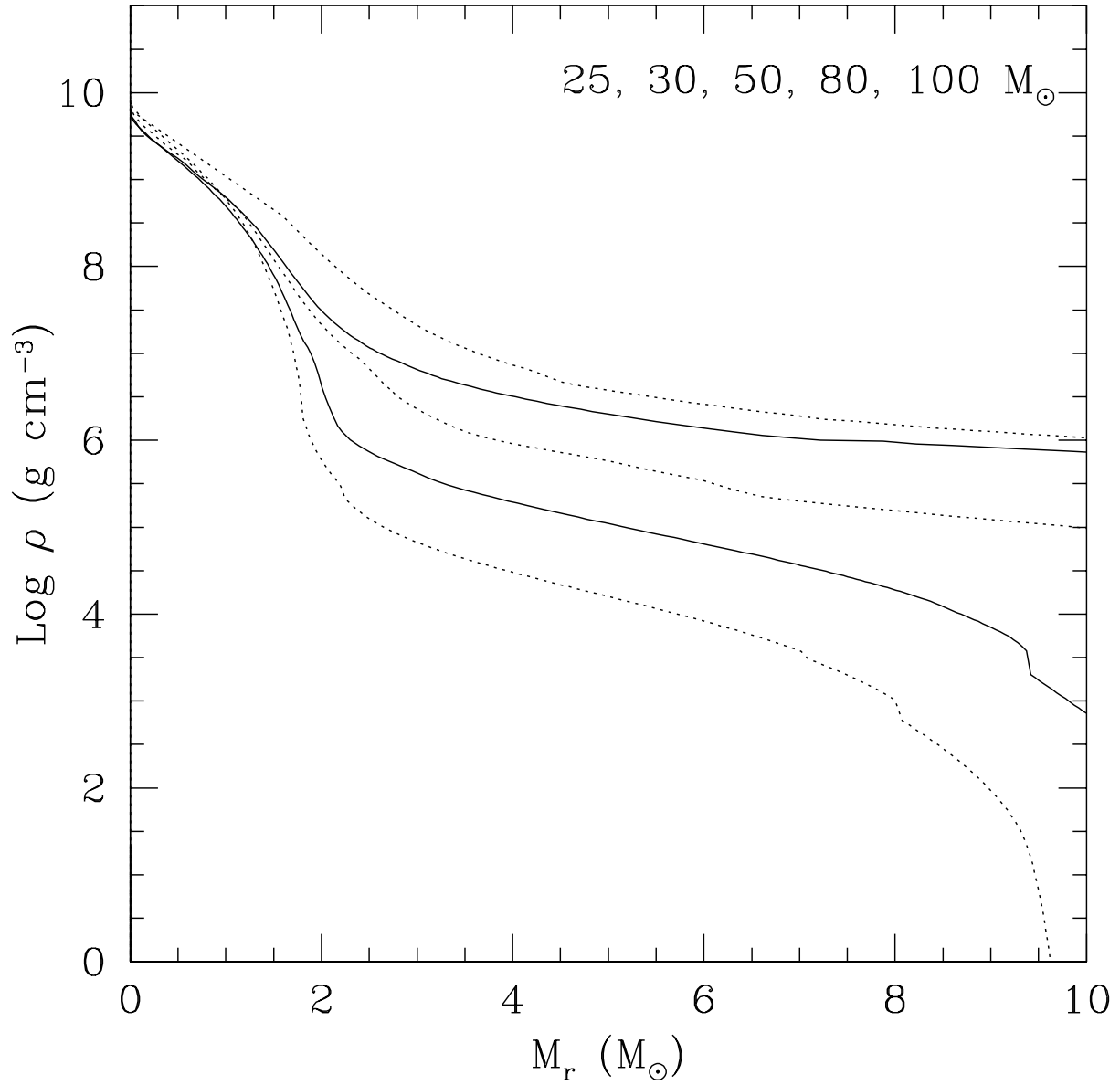


Fig. 3.— The enclosed mass (M_r) - density (ρ) relation of our pre-SN progenitors. The masses of the models are 25, 30, 50, 80, and 100 M_{\odot} , from bottom to top respectively.

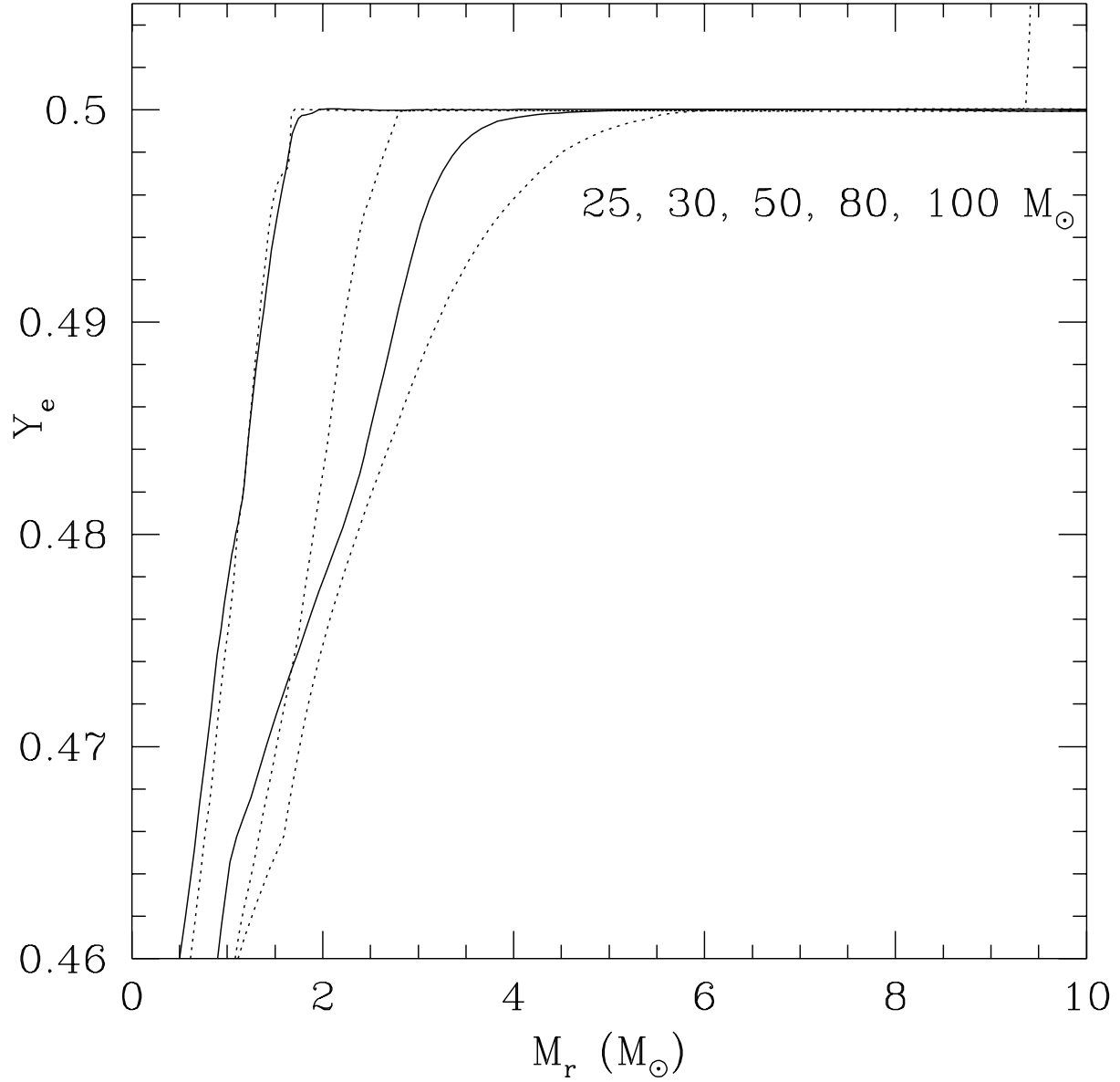


Fig. 4.— The enclosed mass (M_r) - electron mole fraction (Y_e) relation of our pre-SN progenitors. The masses of the models are 25, 30, 50, 80, and 100 M_{\odot} , from left to right respectively. Solid lines represent 30 and 80 M_{\odot} models.

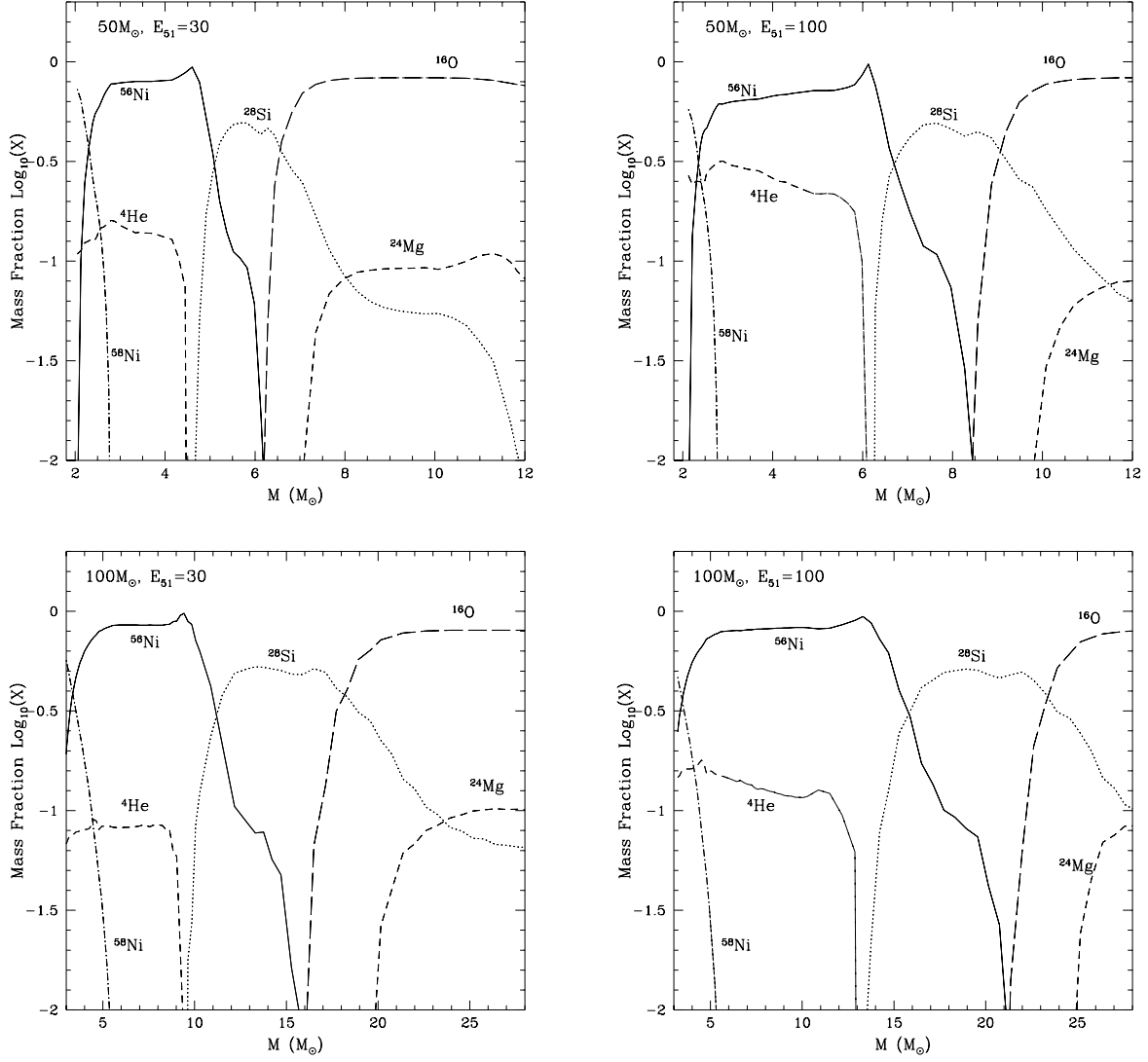


Fig. 5.— The post-explosion abundance distributions for the 50M_⊙ models (upper two panels) and 100M_⊙ models (lower two panels) when the explosion energy is E₅₁ = 30 (left) and E₅₁ = 100 (right.)

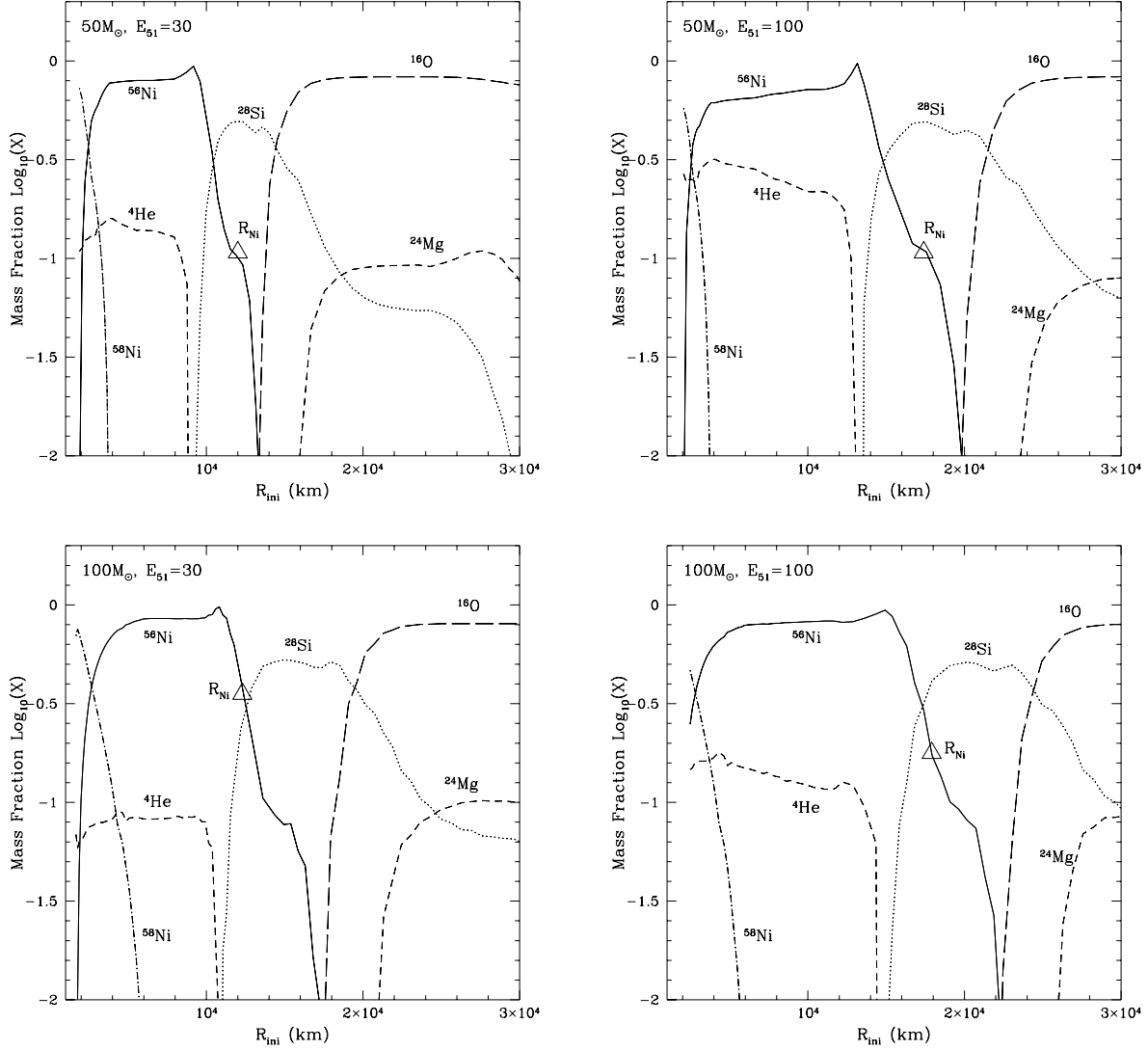


Fig. 6.— Same as Figures 5 but the horizontal axis is replaced by the radius of the progenitor, R_{ini} (km). The location of R_{Ni} calculated by the equation (1) are also shown by large triangles. Here, we note that R_{Ni} appears to be a little over-estimated because the temporal energy absorption due to the matter dissociation is not taken into account in the equation (1).

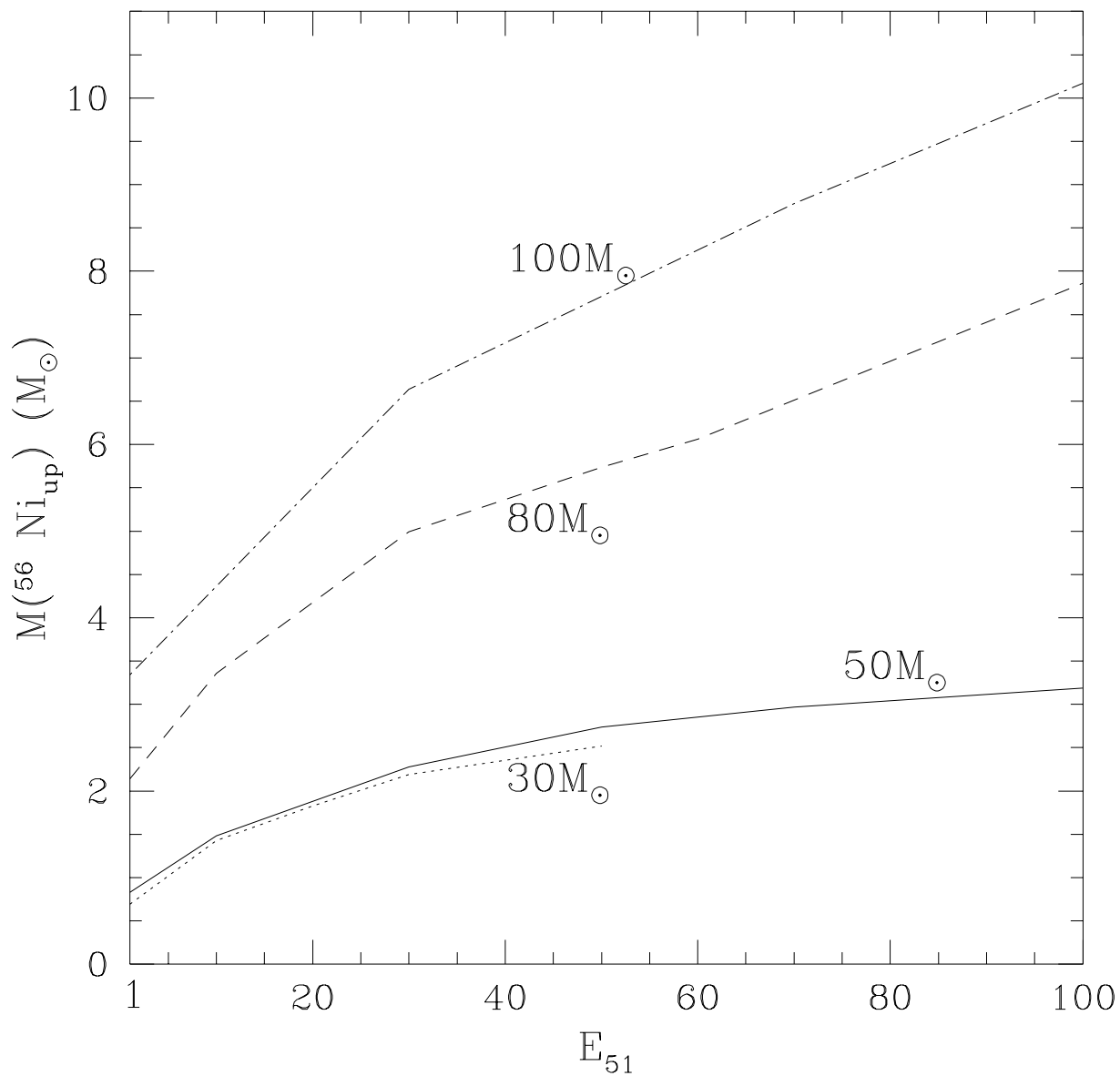


Fig. 7.— The upper limit of ^{56}Ni masses produced by core-collapse SNe with various masses and explosion energies. $^{56}\text{Ni}_{\text{up}}$ shown here are the ejected ^{56}Ni mass when the mass-cut is located at the top of the Fe-core. If mass-cut is larger the ejected mass will be smaller.